Nanoscale

Accepted Manuscript

This article can be cited before page numbers have been issued, to do this please use: K. Liu, F. Wang, T. A. Shifa, Z. Wang, K. Xu, Y. Zhang, Z. Cheng, X. Zhan and J. He, *Nanoscale*, 2017, DOI: 10.1039/C7NR00460E.

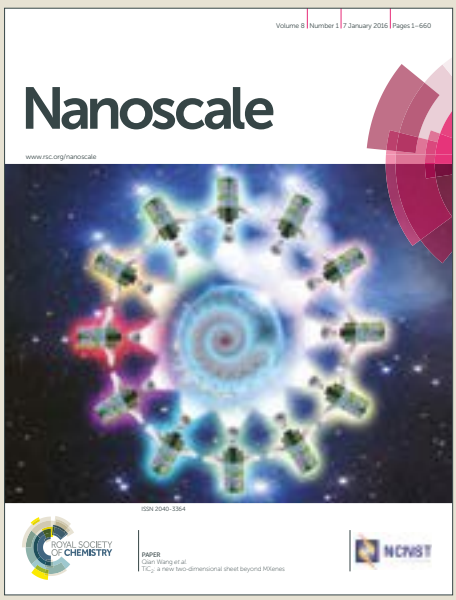

ROYAL SOCIETY OF CHEMISTRY

rsc.li/nanoscale

View Article Online
DOI: 10.1039/C7NR00460E

Nanoscale

ARTICLE

An Efficient Ternary $CoP_{2x}Se_{2(1-x)}$ Nanowire Array for overall Water Splitting

Received 00th January 20xx,
Accepted 00th January 20xx

DOI: 10.1039/x0xx00000x

www.rsc.org/

Kaili Liu[a,b,c], Fengmei Wang[a,b], Tofik Ahmed Shifa[a,b], Zhenxing Wang[a], Kai Xu[a,b], Yu Zhang[a], Zhongzhou Cheng[a,d], Xueying Zhan[a] and Jun He[a]*

Developing earth-abundant and efficient bifunctional electrocatalysts for realizing hydrogen evolution reaction (HER) and oxygen evolution reaction (OER) in alkaline condition is an intriguing challenge. Here, a ternary necklace-like $CoP_{2x}Se_{2(1-x)}$ nanowire arrays are synthesized *via* simultaneously phosphorizing and selenizing $Co(OH)_2$ nanowires. Owing to the substitution of P atom in the ternary system, the optimal electronic structure of the $CoP_{2x}Se_{2(1-x)}$ can be obtained and the stability can also be enhanced for hydrogen evolution. Thus, the ternary $CoP_{2x}Se_{2(1-x)}$ NWs is highly active for electrochemical hydrogen evolution in both acidic and alkaline media, achieving a current density of 10 mA cm^{-2} at overpotentials of 70 mV and 98 mV, respectively. To realize the overall water splitting, we further illustrated the experiment by using the $CoP_{2x}Se_{2(1-x)}$ NWs as cathode and $Co(OH)_2$ NWs as anode, which requires a cell voltage of 1.65 V to afford a water splitting current density of 10 mA cm^{-2} in strong alkaline media (1.0 M KOH).

Introduction

Compared with fossil fuels, hydrogen energy is one of the promising alternatives for renewable fuel due to its sustainable and environmentally friendly characteristics.[1-7] Electrocatalytic water splitting is an efficient route to produce pure hydrogen and oxygen gas. Typically, it is composed of hydrogen evolution reaction (HER, $2H^+ + 2e^- \rightarrow H_2$) in cathode electrode and oxygen evolution reaction (OER, $2H_2O \rightarrow 4e^- + 4H^+ + O_2$) in anode electrode.[8-10] To date, Pt-based and Ir/Ru-based materials are regarded as the benchmarks for HER and OER, respectively. Unfortunately, their high cost hinders the practical application in large-scale. It is, thus, extremely urgent to develop inexpensive and earth-abundant alternative electrocatalysts. In the last few years, great efforts have been made in developing non-noble metal catalysts, including transition metal chalcogenides,[11-19] phosphides,[20-24] and carbides[25, 26] for HER, as well as transition metal phosphate,[27] oxides[28-31] and hydroxides[32-35] for OER. Notably, overall water splitting must be operated in the same electrolyte in the practical process.[36] What's more, water splitting conducted in alkaline solution has emerged as a much more effective method for commercial hydrogen production due to the scare electrocatalyst and much more energy-intensive of OER in acidic media.[37, 38] Therefore, it's attractive to develop novel non-noble bifunctional electrocatalysts with high activity and stability for overall water splitting in alkaline solution.

Nowadays, transition metal dichalcogenides (TMDs) such as $NiSe_2$[39] and CoS_2[40, 41] and transition metal phosphides (TMPs) like CoP,[21, 42, 43] FeP,[44] and $Ni_{12}P_5$[45] have been extensively developed for HER with high performance and stability in both acidic and basic media due to their excellent catalytic performance and high stability. Unlike the binary materials, component controllably synthesized ternary materials, such as $WS_{2(1-x)}Se_{2x}$,[46] $MoS_{2(1-x)}Se_{2x}$,[47] CoPS,[48, 49] NiP_xSe_{2-x}[50] and $CoS_{2x}Se_{2(1-x)}$[51] are found to require a much lower overpotentials. Encouraged by this and considering the fact that substitution of the P atom in $CoSe_2$ would tangibly modify the electronic structure of the resulting ternary material, we designed a rational synthesis of $CoP_{2x}Se_{2(1-x)}$. Benefitting from the advantage of the controllability of our method, the optimum P to Se ratio can improve the activity and stability via tailoring the electronic structure and allowing the exposure of more active sites. It is therefore reasonable to predict that $CoP_{2x}Se_{2(1-x)}$ could be a promising candidate for HER.

Herein, we successfully synthesize the ternary necklace-like $CoP_{2x}Se_{2(1-x)}$ nanowire arrays, which provide much more electrochemical active area, on carbon fiber *via* phosphorization and selenization reaction. Being an electrocatalyst for HER in acidic media, the $CoP_{2x}Se_{2(1-x)}$ electrode achieves current density of 10 mA cm^{-2} at overpotential of 70 mV in acidic solution and shows high stability. Significantly, the $CoP_{2x}Se_{2(1-x)}$ electrode also exhibits excellent electrocatalytic activity and durability in alkaline

[a] CAS Center for Excellence in Nanoscience, CAS Key Laboratory of Nanosystem and Hierarchical Fabrication National Center for Nanoscience and Technology, Beijing 100190, China
[b] University of Chinese Academy of Science, No.19AYuquan Road, Beijing 100049, China.
[c] Sino-Danish Center for Education and Research, Beijing, 100190, China.
[d] School of Materials Science and Engineering, University of Science and Technology Beijing, Beijing 100083, China.

Electronic Supplementary Information (ESI) available: SEM and TEM images of $Co(OH)_2$ and $CoP_{2x}Se_{2(1-x)}$ NWs.. See DOI: 10.1039/x0xx00000x

View Article Online
DOI: 10.1039/C7NR00460E

condition. It needs only 98 mV to reach current density of 10 mA cm^{-2} which is very close to the HER performance in acidic solution. Furthermore, to realize a practical utilization, we designed overall water splitting setup in such a way that the $CoP_{2x}Se_{2(1-x)}$ NWs and $Co(OH)_2$ NWs served as cathode and anode, respectively. Accordingly, this configuration requires a cell voltage of 1.65 V to reach a current density of 10 mA cm^{-2}, suggestive of its promising feature for practical realization of water splitting.

Experimental section

Synthesis of $Co(OH)_2$ NWs

The $Co(OH)_2$ nanowires on a CF was synthesized by a method that we have reported in our previous work.[52] First, the CFs were ultrasonically washed by acetone, ethanol and ultrapure water in sequence, and then dried at 60 °C. Subsequently, 1.90 g $CoCl_2{\cdot}6H_2O$, 2.424 g $CO(NH_2)_2$ were dissolved in 40 mL ethanol for 10 min. To form a seed layer on CFs, the soaked CFs were calcined at 450 °C for 4 h under an argon flow. Then, 1.90 g $CoCl_2{\cdot}6H_2O$ and 2.424 g $CO(NH_2)_2$ were dissolved in 40 mL ultrapure water. After transferring the solution into a 50 mL Teflon-lined stainless steel autoclave, one piece of the seeded CFs was immersed in the solution. The autoclave was then heated in an electrical oven at 90 °C for 4 h. After cooling down to room temperature, the obtained $Co(OH)_2$ NWs washed with water and ethanol. Eventually, the $Co(OH)_2$ NWs dried at 60 °C for further use.

Synthesis of $CoP_{2x}Se_{2(1-x)}$ NWs

A horizontal quartz tube furnace is utilized to convert the $Co(OH)_2$ NWs into $CoP_{2x}Se_{2(1-x)}$ NWs. The $Co(OH)_2$ NWs on CF was placed at the downstream side of the furnace and a mixture of phosphorus and selenium powder was placed at the upstream side of the furnace. At the beginning, the tube furnace was flushed under a 100 sccm Ar flow for three times to create an oxygen-free environment. Subsequently, the zones of the substrate and powder were quickly heated to 450 °C and 270 °C in 20 min, respectively. The reaction temperature maintained for 60 min to fully convert the $Co(OH)_2$ NWs into $CoP_{2x}Se_{2(1-x)}$ NWs, followed by natural cooling down. During the synthesis process, the flow of Ar is kept at a rate of 100 sccm.

Characterizations

The morphologies of $Co(OH)_2$ NWs and $CoP_{2x}Se_{2(1-x)}$ NWs were characterized by Hitach S-4800 scanning electron microscopy (SEM) under 20 kV and TecnaiF20 transmission electron microscopy (TEM) at 200 kV. STEM-EDX elemental mapping was characterized by TecnaiF20 and the energy dispersive X-ray spectroscopy (EDX) was performed on Hitach S-4800. X-ray diffraction (XRD) patterns (Philips X'Pert Pro Super) were obtained using Cu Kα radiation (λ = 1.5418 Å) and X-ray photoelectron spectroscopy (XPS) was tested on ESCALAB250Xi. The pH of the electrolyte was performed by the METTLER TOLEDO pH meter (FE20).

Electrochemical measurements

The test for hydrogen evolution reaction (HER) and the oxygen evolution reaction (OER) were performed in a typical three-electrode configuration at an electrochemical station (CHI 660D). The HER measurements were conducted in 0.5 M H_2SO_4 (pH=0.69) and 1M KOH solution (pH=13.71). When 0.5 M H_2SO_4 solution was used as electrolytes in the three-electrode system, the CF covered with $CoP_{2x}Se_{2(1-x)}$ NWs used as the working electrode (WE) and a platinum wire and a saturated calomel electrode (SCE) served as the counter electrode (CE) and reference electrode (RE), respectively. In acidic media, the equation E (RHE) = E (SCE) + 0.242 + 0.059 pH is considered. Linear sweep voltammetry (LSV) measurements were measured at a scan rate of 5 mV s^{-1} from +0.1 to -0.4V *vs.* reversible hydrogen electrode (RHE). To estimate the double-layer capacitance, cyclic voltammetry (CV) experiments were performed from 0 to +0.1 V *vs.* RHE with various scan rates (20-200 mV/s). We used a mercuric oxide electrode (MOE) as RE when HER measurements were tested in 1 M KOH solution. In alkaline media, the equation E (RHE) = E (MOE) + 0.098 + 0.059 pH is considered. LSV measurements were tested from +0.1 to -0.4V *vs.* RHE at a scan rate of 2 mV/s. CV experiments were performed from +0.05 to +0.15 V *vs.* RHE with different values of scan rates (20-200 mV/s) to assess the double-layer capacitance. The OER measurements were measured in 1 M KOH using the CF covered with $CoP_{2x}Se_{2(1-x)}$ NWs as the WE, a platinum wire as the CE and a MOE as the RE. LSV was conducted from 1.0 to 1.8 V *vs.* RHE at a scan rate of 2 mV s^{-1}. The overall water splitting was evaluated in 1 M KOH using a two-electrode configuration. The $CoP_{2x}Se_{2(1-x)}$ NWs on CF served as the cathode for HER, and $Co(OH)_2$ on CF used as anode for OER. The polarization curve was performed at a scan rate of 2 mV s^{-1}. All the potentials were calibrated to a RHE and all polarization curves were corrected for *iR* losses.

Results and discussion

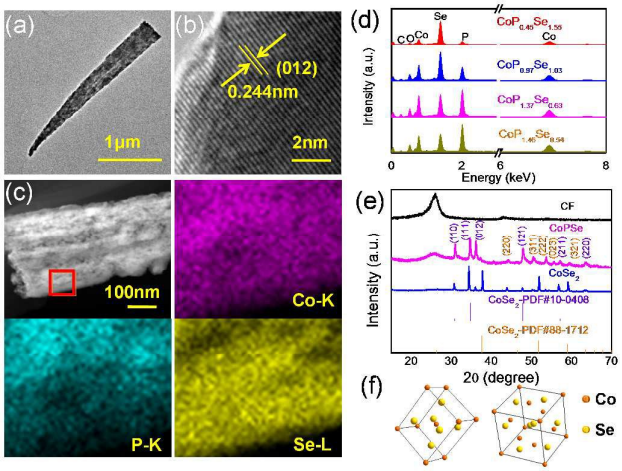

Fig. 1. TEM image (a), HRTEM image (b),STEM image and EDX elemental mapping(c) of a $CoP_{2x}Se_{2(1-x)}$ NW. (d) EDX spectra of $CoP_{0.45}Se_{1.55}$, $CoP_{0.97}Se_{1.03}$, $CoP_{1.37}Se_{0.63}$ and $CoP_{1.46}Se_{0.54}$. (e) XRD patterns of bare CF, $CoSe_2$ NWs and $CoP_{2x}Se_{2(1-x)}$ NWs. (f) The orthorhombic macarsite-type structure (left) and cubic pyrite-type

View Article Online
DOI: 10.1039/C7NR00460E

structure (right) of $CoSe_2$ and Co and Se are exhibited in blue and red, respectively.

The ternary $CoP_{2x}Se_{2(1-x)}$ NWs were prepared through selenizing and phosphorizing $Co(OH)_2$ NWs, simultaneously. (see the Experimental Section).[51, 52] In general, we first grew $Co(OH)_2$ NWs (Fig. S1a-b), which is utilized as the precursor for achieving $CoP_{2x}Se_{2(1-x)}$ NWs (Fig. S2a and b), on carbon fiber (CF) through hydrothermal method. Scanning electron microscopy (SEM) and transmission electron microscope (TEM) were used to observe the morphologies of $Co(OH)_2$ NWs (Fig. S1a-b) and $CoP_{2x}Se_{2(1-x)}$ NWs. Low magnification TEM (Fig. 1a) reveals that the diameter of the $CoP_{2x}Se_{2(1-x)}$ NW is around 200 nm with the length of several micrometers. Different with the smooth surface of $Co(OH)_2$ NWs (Fig. S1b), the resulting $CoP_{2x}Se_{2(1-x)}$ NWs have a rough surface (Fig. 1a) with the necklace-like morphology. Moreover, the high-resolution TEM (HRTEM) image in Fig. 1b demonstrates the lattice fringes with the interplanar spacing of 0.244 nm, which belongs to crystal plane of (012). The scanning TEM (STEM) image and the corresponding energy-dispersive X-ray (EDX) elemental mapping images (Fig. 1c) further reveals that the Co, P and Se are distributed uniformly in the $CoP_{2x}Se_{2(1-x)}$ NW. Furthermore, the composition of the $CoP_{2x}Se_{2(1-x)}$ NW can be controlled through varying the ratios of P and Se. The EDX spectra (Fig. 1d) indicate the presence of cobalt, phosphorus and selenium in elemental compositions of $CoP_{0.45}Se_{1.55}$, $CoP_{0.97}Se_{1.03}$, $CoP_{1.37}Se_{0.63}$ and $CoP_{1.46}Se_{0.54}$. And the X-ray diffraction (XRD) patterns of bare CF, $CoSe_2$ NWs and $CoP_{2x}Se_{2(1-x)}$ NWs are presented in Fig. 1e. In comparison with that of $Co(OH)_2$ (Fig. S1c), there are no diffraction peaks meant for $Co(OH)_2$ in $CoP_{2x}Se_{2(1-x)}$, demonstrating a successful our conversion process and further verifying the EDX results. It is notable that all the diffraction peaks of $CoP_{2x}Se_{2(1-x)}$ shift to a higher degree, compared with the XRD pattern of pristine $CoSe_2$, owing to the smaller size of phosphorus atom as compared to selenium atom. The similarity of the XRD patterns of $CoP_{1.37}Se_{0.63}$ and $CoSe_2$ suggests that P atom substituted Se atom during the CVD process. Remarkably, we observed that the XRD pattern of $CoSe_2$ is consistent with orthorhombic marcasite-structural phase (PDF# 10-0408) (Fig. 1f left) and cubic pyrite-structural phase (PDF# 88-1712) (Fig. 1f right), indicating that the $CoP_{2x}Se_{2(1-x)}$ NWs consist of those two phases. To further confirm the chemical composition of $CoP_{2x}Se_{2(1-x)}$, we also conducted X-ray photoelectron spectroscopy (XPS) analysis. Fig. 2a shows that the two peaks for Co $2p_{3/2}$ and $2p_{1/2}$ are located at binding energies of 779.05 eV and 794.01 eV. And the peaks of Se $3d_{5/2}$ and Se $3d_{3/2}$ are located at 54.55 eV and 55.36 eV, respectively (Fig. 2b). Compared with the reported data of Co and Se in binary $CoSe_2$,[53] this results show a very slight shift due to the incorporation of P element. The deconvulated P 2p spectrum presents two peak regions (Fig. 2c). One of the regions has two peaks with one located at the binding energy of 129.60 eV and the other at 130.1 eV (P $2p_{3/2}$ and $2p_{1/2}$), which corresponds to phosphorus anions. The second region is centred at 133.6 and 135.5 eV (unresolved doublet) and these two peaks can be assigned to the phosphate-like P. This is agree with the reported results.[49] Meanwhile, the quantitative analysis also shows that the ratio of P and Se is near to 2 : 1 and this result is consistent with the EDX data.

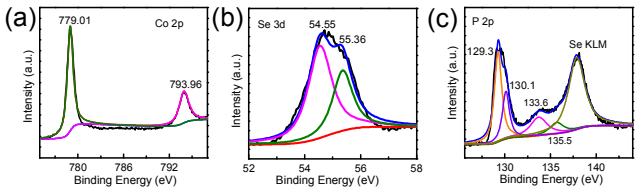

Fig. 2. XPS spectra of (a) Co 2p, (b) Se 3d and (c) P 2p region.

The HER activity of $CoP_{2x}Se_{2(1-x)}$ NWs was evaluated in 0.5 M H_2SO_4 electrolyte using a typical three-electrode setup at room temperature. The $CoP_{2x}Se_{2(1-x)}$ NWs on CF was directly employed as the working electrodes, a Pt wire and a saturated calomel electrode (SCE) used as counter electrode (CE) and reference electrode (RE), respectively. As comparison, bare CF and Pt electrodes were also measured under the same condition. In order to reflect the intrinsic activity of the catalysts, all initial data are presented after *iR* correction.[54] Fig. 3a shows the polarization curves of $CoP_{1.37}Se_{0.63}$ NWs, bare CF and Pt with a scan rate of 5 mV s^{-1}. The bare CF shows poor HER activity in the measurement potential, indicating its negligible contribution towards hydrogen evolution reaction (HER). The $CoP_{1.37}Se_{0.63}$ NWs requires an overpotential of 70 mV *vs.* reversible hydrogen electrode (RHE) to achieve the current density of 10 mA cm^{-2}, which is close to that of Pt foil (39 mV at 10 mA cm^{-2}). What's more, this performance is more superior than some reported results among binary cobalt-based electrocatalysts like $CoSe_2$ nanoparticles,[53] $CoSe_2$ NW/CC[55] and CoS_2 NW,[56] as well as our reported ternary $CoS_{2x}Se_{2(1-x)}$ NWs (Table S1).[51] We also compared the HER activity of $CoP_{2x}Se_{2(1-x)}$ NWs with other samples with different atomic ratios ($CoSe_2$, $CoP_{0.45}Se_{1.55}$, $CoP_{0.97}Se_{1.03}$ and $CoP_{1.46}Se_{0.54}$) (Fig. S3 and Fig. S4a). The overpotential of $CoP_{1.37}Se_{0.63}$ NWs grown on CFs at a catalytic current density of 10 mA cm^{-2} is lowest among the samples with various atomic ratios (Fig. 3b), implying the best HER performance of $CoP_{1.37}Se_{0.63}$ NWs. In order to assess the kinetics of the electrodes, Tafel plots of $CoP_{1.37}Se_{0.63}$ NWs, Pt (Fig. 3c), $CoP_{0.45}Se_{1.55}$, $CoP_{0.97}Se_{1.03}$, $CoP_{1.37}Se_{0.63}$ and $CoP_{1.46}Se_{0.54}$ (Fig. S4b) were extracted from their corresponding polarization curves. Accordingly, the Tafel plots (Fig. 3c) of $CoP_{1.37}Se_{0.63}$ NWs is found to be 54 mV $decade^{-1}$. However, $CoP_{0.45}Se_{1.55}$ NWs, $CoP_{0.97}Se_{1.03}$ NWs and $CoP_{1.46}Se_{0.54}$ NWs demonstrate higher Tafel slopes of 64, 59 and 61 mV $decade^{-1}$, respectively. One of the reasonable explanations for the superior HER performance of $CoP_{1.37}Se_{0.63}$ NWs is that the incorporation of P into $CoSe_2$ expectedly endows such material a unique electronic structure which would facilitate the hydrogen evolution. For cobalt dichalcogenide, the most important factor for the density of states in the conduction band is d-electron filling in e_g orbitals,[8, 57] which plays an important role on the adsorption of H atom. The doping of P atom contributes to the partially filled e_g orbital which would facilitate the electrocatalytic activity.[58] Another important parameter to assess the HER performance is the electrochemically active surface area. As the electrochemical double-layer capacitance, C_{dl}[53] can be used to determine the active surface area, cyclic voltammogram (CV) curves of various electrocatalysts were performed from 0 to 0.1 V *vs.* RHE at various scan rates (20 mV s^{-1} to 200 mV s^{-1}) (Fig. S5a–b). As shown in Fig. S5c, the C_{dl} of $CoP_{1.37}Se_{0.63}$ NWs is 23.3 mF cm^{-2} which is much higher than the

View Article Online
DOI: 10.1039/C7NR00460E

binary $CoSe_2$ NWs (7.48 mF cm $^{-2}$), indicating the increased electrochemically active surface area of ternary $CoP_{1.37}Se_{0.63}$ NWs. The morphology of $CoSe_2$ NWs and ternary $CoP_{1.37}Se_{0.63}$ NWs are similar, thus the increase in C_{dl} can be associated to the proliferation of active sites on the $CoP_{1.37}Se_{0.63}$ NWs, which is consistent with some reported results.[59] Moreover, the stability of $CoP_{1.37}Se_{0.63}$ NWs was investigated with chronoamperometric measurement. Fig. 3d shows that the decrease of catalytic current density is negligible for up to 12 h of electrolysis, indicating the good stability of the $CoP_{1.37}Se_{0.63}$ NWs for HER in acid solution. The SEM image and XRD pattern (Fig. S6a and Fig. S7) of the $CoP_{1.37}Se_{0.63}$ NWs after the stability measurement also verify the robustness of $CoP_{1.37}Se_{0.63}$ NWs.

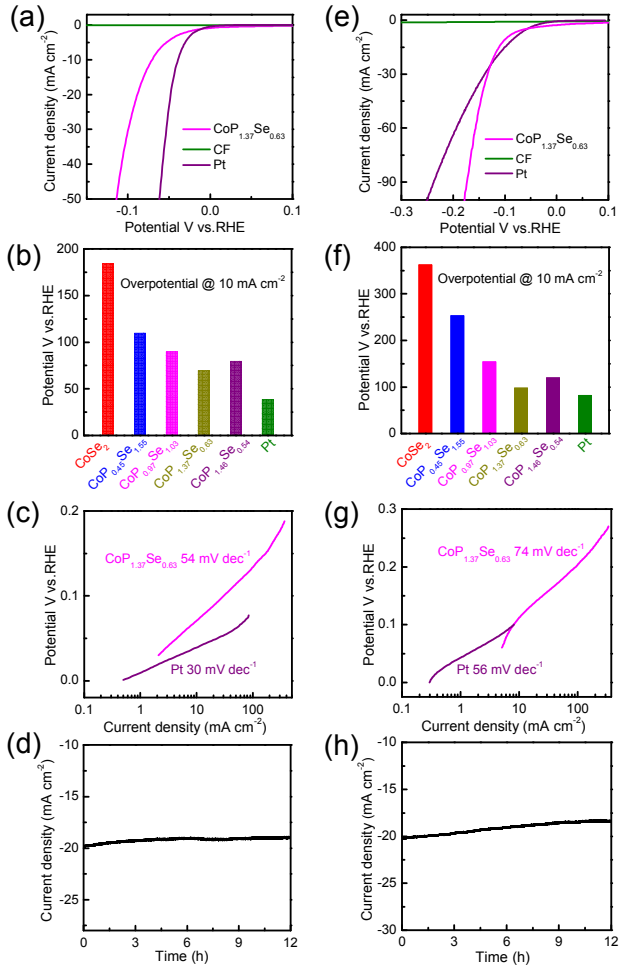

Fig. 3. Polarization curves of $CoP_{1.37}Se_{0.63}$ NWs, bare CF and Pt foil for HER in 0.5 M H_2SO_4 (a) and 1 M KOH (e). Comparison of the overpotentials of the different $CoP_{2x}Se_{2(1-x)}$ electrodes and Pt foil at the current density of 10 mA cm^{-2} for HER in 0.5 M H_2SO_4 (b) and 1 M KOH (f). The corresponding Tafel plots of $CoP_{1.37}Se_{0.63}$ NWs and Pt foil in 0.5 M H_2SO_4 (c) and 1 M KOH (g). Chronoamperometric curve of $CoP_{1.37}Se_{0.63}$ NWs at a constant potential in 0.5 M H_2SO_4 (d) and 1 M KOH (h).

We further evaluated the HER activity of $CoP_{1.37}Se_{0.63}$ NWs in strong basic media (1M KOH) wherein a mercuric oxide electrode (MOE) served as reference electrode. Fig. 3e exhibits the HER activity of $CoP_{1.37}Se_{0.63}$ NWs with the overpotential of 98 mV at 10 mA cm $^{-2}$ in alkaline condition is very similar to that of Pt foil (82 mV at 10 mA cm $^{-2}$). The HER performance of the $CoP_{1.37}Se_{0.63}$ NWs is also better than some reported binary Co-based materials.[40, 43, 60] In comparison with $CoSe_2$ (Fig. S3), $CoP_{0.45}Se_{1.55}$, $CoP_{0.97}Se_{1.03}$ and $CoP_{1.46}Se_{0.54}$ (Fig. S4c), $CoP_{1.37}Se_{0.63}$ NWs exhibits the best HER activity in alkaline solution. As shown in Fig. 3f, the overpotential required to achieve a current density of 10 mA cm $^{-2}$ for $CoP_{1.37}Se_{0.63}$ NWs is much lower than $CoSe_2$ (362mV), $CoP_{0.45}Se_{1.55}$ (253 mV), $CoP_{0.97}Se_{1.03}$ (154 mV) and $CoP_{1.46}Se_{0.54}$ (120mV), indicating that the $CoP_{1.37}Se_{0.63}$ NWs is the optimal one for HER in alkaline media. The comparison of the corresponding Tafel slopes of various atomic ratios of P to Se in $CoP_{2x}Se_{2(1-x)}$ further suggests that the $CoP_{1.37}Se_{0.63}$ NWs shows the optimal performance for HER in basic solution. The cyclic voltammogram (CV) curves of $CoP_{1.37}Se_{0.63}$ NWs, $CoSe_2$ NWs between 0.05 and 0.15 V *vs.* RHE with different values of scan rates (10 mV s $^{-1}$ to 100 mV s $^{-1}$) in alkaline condition (Fig. S5d–e) were conducted. According to Fig. S4f, the C_{dl} of $CoP_{1.37}Se_{0.63}$ NWs and $CoSe_2$ NWs are 20.2 mF cm $^{-2}$ and 5.7 mF cm $^{-2}$, respectively. This result shows a consistent trend with the one in acidic media. The $CoP_{1.37}Se_{0.63}$ NWs also exhibits excellent stability in alkaline solution (Fig. 3f). After 12 h of electrolysis, there is only a minor deterioration of catalytic current density. The SEM image and XRD pattern of $CoP_{1.37}Se_{0.63}$ NWs after HER test show that our electrodes are stable in strong alkaline solution. In general, the excellent HER performance and good stability of $CoP_{1.37}Se_{0.63}$ NWs make it an ideal HER catalyst in both acidic and alkaline solutions.

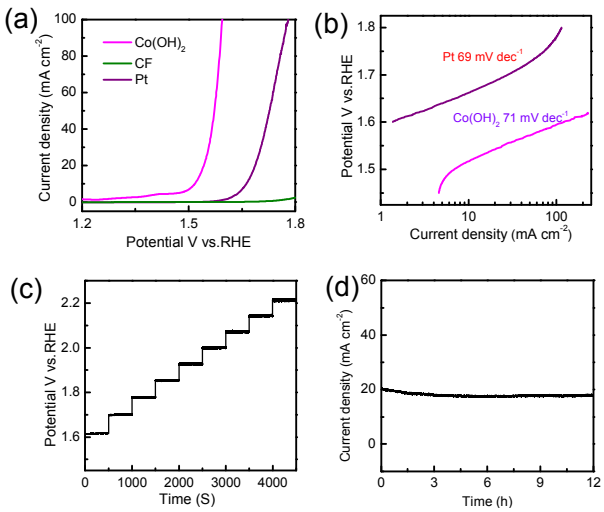

Fig. 4 (a) Polarization curves of $Co(OH)_2$ NWs, bare CF and Pt for OER. (b) The corresponding Tafel plots of $Co(OH)_2$ NWs and Pt. (c) Multi-current process of $CoP_{1.37}Se_{0.63}$ NWs. The current density started at 50 mA cm $^{-2}$ and finished at 450 mA cm $^{-2}$, with an increment of 50 mA cm $^{-2}$ per 500 s without iR correction. (d) Chronoamperometric curve of $Co(OH)_2$ NWs at constant potential for OER. All experiments were performed in 1.0 M KOH.

We then assessed the OER activity for $Co(OH)_2$ NWs in alkaline solution. As an OER electrode, the $Co(OH)_2$ NWs requires an overpotential of 290 mV to achieve a catalytic current density of 10 mA cm $^{-2}$ and its OER performance is even better than Pt (Fig. 4a). The corresponding Tafel slope of $Co(OH)_2$ NWs is 71 mV dec $^{-1}$ (Fig. 4b), which is smaller than most of the reported metal hydroxide,

View Article Online
DOI: 10.1039/C7NR00460E

verifying a favorable OER kinetics for $Co(OH)_2$ NWs. Fig. 4c shows a multi-step chronopotentiometric curve for $Co(OH)_2$ NWs in 1.0 M KOH. The current is increased from 50 to 450 mA cm^{-2} and remains 500s for each increment of 50 mA cm^{-2}. The potential immediately levels off at 1.62 V at the start current of 50 mA cm^{-2} and remains steady for the rest 500 s and the other steps also show similar results, indicating the excellent mass transportation and mechanical robustness of the $Co(OH)_2$ NWs. The time-dependent current density curve (Fig. 4d) was also studied to probe the long-term stability of $Co(OH)_2$ NWs. According to Fig. 4d, there is no obvious current density change for up to 12 hours OER test, implying the excellent stability of $Co(OH)_2$ NWs for OER in strong alkaline solution.

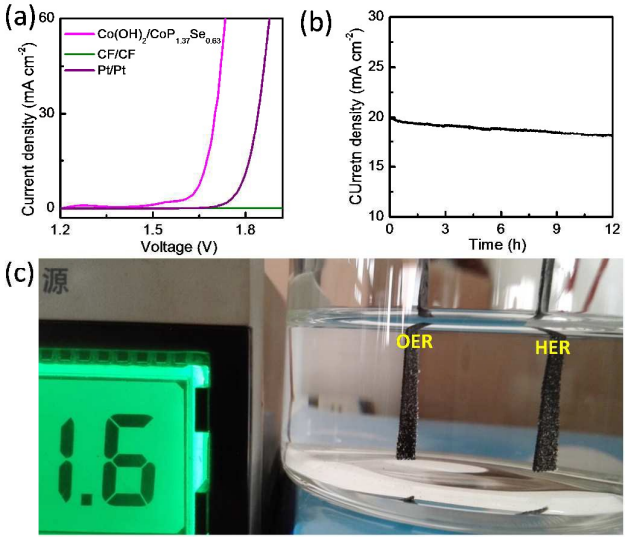

Fig. 5 (a) Polarization curves for overall water splitting of $Co(OH)_2/CoP_{1.37}Se_{0.63}$, CF/CF and Pt/Pt in a two-electrode configuration with a scan rate of 2 mV s^{-1}. (b) Chronoamperometric curve for overall water splitting of $Co(OH)_2/CoP_{1.37}Se_{0.63}$ in a two two-electrode system at a constant potential. (d) Optical photograph of overall water splitting device powered by a constant voltage of 1.6 V.

Encouraged by excellent HER performance of $CoP_{1.37}Se_{0.63}$ NWs as well as good OER activity of $Co(OH)_2$ NWs in alkaline conditions, the overall electrochemical water splitting in a strong alkaline solution (1.0 M KOH) is further conducted using a two-electrode setup with $CoP_{1.37}Se_{0.63}$ NWs and $Co(OH)_2$ NWs served as cathode and anode ($CoP_{1.37}Se_{0.63}/Co(OH)_2$), respectively. Fig. 5a exhibits that $CoP_{1.37}Se_{0.63}/Co(OH)_2$ needs a voltage of 1.65 V to achieve a current density of 10 mA cm^{-2} which is much smaller than Pt (1.81V). We further examined the long-term electrochemical stability of $CoP_{1.37}Se_{0.63}/Co(OH)_2$ (Fig. 5b). Accordingly, there is no obvious change in the current density with in 12 hours test for overall water splitting in 1.0 M KOH, suggesting the excellent stability of $CoP_{1.37}Se_{0.63}/Co(OH)_2$. Fig. 5c presents a photograph to illustrate that an voltage of 1.6V can drive overall water splitting with a large amount of H_2 bubbles on the cathode and O_2 bubbles on the anode, confirming the high performance of the $CoP_{1.37}Se_{0.63}/Co(OH)_2$.

Conclusions

In summary, ternary $CoP_{2x}Se_{2(1-x)}$ NW arrays on carbon fiber was successfully fabricated *via* simultaneous phosphorization and selenization of $Co(OH)_2$ NWs. The $CoP_{2x}Se_{2(1-x)}$ NWs can be directly used as an excellent and durable electrode for HER under both acidic and alkaline conditions. After optimizing the composition, $CoP_{1.37}Se_{0.63}$ NWs can afford a current density of 10 mA cm^{-2} for HER at 70 mV and 98 mV in acidic and alkaline media, respectively. Furthermore, the $Co(OH)_2$ NWs also shows markedly high and stable catalytic activity toward OER in alkaline solution and requires only 290 mV to reach a current density of 10 mA cm^{-2}. The overall electrochemical water splitting in a strong alkaline solution (1.0 M KOH) is further conducted with $CoP_{1.37}Se_{0.63}$ NWs as cathode and $Co(OH)_2$ NWs as anode. This setup requires a voltage of 1.65 V to generate 10 mA cm^{-2} water-splitting current density. Our work offers an earth-abundant, binding-free material and efficient catalysts for practical overall water splitting in alkaline media.

Acknowledgements

This work was supported by Ministry of Science and Technology of China (No. 2016YFA0200700), National Natural Science Foundation of China (Nos. 21373065, 61474033, 61574050 and 11674072), Strategic Priority Research Program of the Chinese Academy of Sciences (Grant No. XDA09040201) and CAS Key Laboratory of Nanosystem and Hierarchical Fabrication. The authors also gratefully acknowledge the support of Youth Innovation Promotion Association CAS.

Notes and references

1. J. Luo, J.-H. Im, M. T. Mayer, M. Schreier, M. K. Nazeeruddin, N.-G. Park, S. D. Tilley, H. J. Fan and M. Grätzel, *Science*, 2014, **345**, 1593-1596.
2. C. He, X. Wu, J. Shen and P. K. Chu, *Nano Lett.*, 2012, **12**, 1545-1548.
3. D. J. Li, U. N. Maiti, J. Lim, D. S. Choi, W. J. Lee, Y. Oh, G. Y. Lee and S. O. Kim, *Nano Lett.*, 2014, **14**, 1228-1233.
4. S. Bai, C. Wang, M. Deng, M. Gong, Y. Bai, J. Jiang and Y. Xiong, *Angew. Chem. Int. Ed.*, 2014, **53**, 12120-12124.
5. L. Liao, J. Zhu, X. Bian, L. Zhu, M. D. Scanlon, H. H. Girault and B. Liu, *Adv. Funct. Mater.*, 2013, **23**, 5326-5333.
6. M. Zeng and Y. Li, *J. Mater. Chem. A*, 2015, **3**, 510-516.
7. M. S. Faber and S. Jin, *Energy Environ. Sci.*, 2014, **7**, 3519-3542.
8. J. Suntivich, K. J. May, H. A. Gasteiger, J. B. Goodenough and Y. Shao-Horn, *Science*, 2011, **334**, 1383-1385.
9. D. Voiry, H. Yamaguchi, J. Li, R. Silva, D. C. Alves, T. Fujita, M. Chen, T. Asefa, V. B. Shenoy and G. Eda, *Nat. Mater.*, 2013, **12**, 850-855.
10. M. G. Walter, E. L. Warren, J. R. McKone, S. W. Boettcher, Q. Mi, E. A. Santori and N. S. Lewis, *Chem. Rev.*, 2010, **110**, 6446-6473.
11. J. Kibsgaard, Z. Chen, B. N. Reinecke and T. F. Jaramillo, *Nat. Mater.*, 2012, **11**, 963-969.
12. C. Tan and H. Zhang, *Chem. Soc. Rev.*, 2015, **44**, 2713-2731.

View Article Online
DOI: 10.1039/C7NR00460E

13. Y. F. Xu, M. R. Gao, Y. R. Zheng, J. Jiang and S. H. Yu, *Angew. Chem. Int. Ed.*, 2013, **52**, 8546-8550.
14.Y.-R. Zheng, M.-R. Gao, Z.-Y. Yu, Q. Gao, H.-L. Gao and S.-H. Yu, *Chem. Sci.*, 2015, **6**, 4594-4598.
15. H. Zhang, B. Yang, X. Wu, Z. Li, L. Lei and X. Zhang, *ACS applied materials & interfaces*, 2015, **7**, 1772-1779.
16. M. S. Faber, M. A. Lukowski, Q. Ding, N. S. Kaiser and S. Jin, *J. Phys. Chem. C Nanomater. Interfaces*, 2014, **118**, 21347-21356.
17. Y. Yin, J. Han, Y. Zhang, X. Zhang, P. Xu, Q. Yuan, L. Samad, X. Wang, Y. Wang, Z. Zhang, P. Zhang, X. Cao, B. Song and S. Jin, *J. Am. Chem. Soc.*, 2016, **138**, 7965-7972.
18. Q. Ding, B. Song, P. Xu and S. Jin, *Chem.*, 2016, **1**, 699-726.
19.H. Zhang, Q. Ding, D. He, H. Liu, W. Liu, Z. Li, B. Yang, X. Zhang, L. Lei and S. Jin, *Energy Environ. Sci.*, 2016, **9**, 3113-3119.
20. E. J. Popczun, J. R. McKone, C. G. Read, A. J. Biacchi, A. M. Wiltrout, N. S. Lewis and R. E. Schaak, *J. Am. Chem. Soc.*, 2013, **135**, 9267-9270.
21. E. J. Popczun, C. G. Read, C. W. Roske, N. S. Lewis and R. E. Schaak, *Angew. Chem. Int. Ed.*, 2014, **126**, 5531-5534.
22. J. Tian, Q. Liu, N. Cheng, A. M. Asiri and X. Sun, *Angew. Chem. Int. Ed.*, 2014, **53**, 9577-9581.
23. Y. Yan, L. Thia, B. Y. Xia, X. Ge, Z. Liu, A. Fisher and X. Wang, *Adv. Sci.*, 2015, **2**.
24. Y. Yan, B. Y. Xia, X. Ge, Z. Liu, A. Fisher and X. Wang, *Chem.-Eur. J.*, 2015, **21**, 18062-18067.
25. W.-F. Chen, J. T. Muckerman and E. Fujita, *Chem. Commun.*, 2013, **49**, 8896-8909.
26. H. Vrubel and X. Hu, *Angew. Chem. Int. Ed.*, 2012, **124**, 12875-12878.
27. M. W. Kanan and D. G. Nocera, *Science*, 2008, **321**, 1072-1075.
28. T. Y. Ma, S. Dai, M. Jaroniec and S. Z. Qiao, *J. Am. Chem. Soc.*, 2014, **136**, 13925-13931.
29. T. Maiyalagan, K. A. Jarvis, S. Therese, P. J. Ferreira and A. Manthiram, *Nat. Commun.*, 2014, **5**.
30. R. D. Smith, M. S. Prévot, R. D. Fagan, Z. Zhang, P. A. Sedach, M. K. J. Siu, S. Trudel and C. P. Berlinguette, *Science*, 2013, **340**, 60-63.
31. Y. Zhu, W. Zhou, Z. G. Chen, Y. Chen, C. Su, M. O. Tadé and Z. Shao, *Angew. Chem. Int. Ed.*, 2015, **54**, 3897-3901.
32. W. D. Chemelewski, H.-C. Lee, J.-F. Lin, A. J. Bard and C. B. Mullins, *J. Am. Chem. Soc.*, 2014, **136**, 2843-2850.
33. X. Long, J. Li, S. Xiao, K. Yan, Z. Wang, H. Chen and S. Yang, *Angew. Chem. Int. Ed.*, 2014, **126**, 7714-7718.
34.F. Song and X. Hu, *J. Am. Chem. Soc.*, 2014, **136**, 16481-16484.
35. L. Trotochaud, S. L. Young, J. K. Ranney and S. W. Boettcher, *J. Am. Chem. Soc.*, 2014, **136**, 6744-6753.
36. X. Zou, X. Huang, A. Goswami, R. Silva, B. R. Sathe, E. Mikmeková and T. Asefa, *Angew. Chem. Int. Ed.*, 2014, **126**, 4461-4465.
37. K. Zeng and D. Zhang, *Prog. Energy Combust. Sci.*, 2010, **36**, 307-326.
38. M. S. Burke, M. G. Kast, L. Trotochaud, A. M. Smith and S. W. Boettcher, *J. Am. Chem. Soc.*, 2015, **137**, 3638-3648.
39. H. Liang, L. Li, F. Meng, L. Dang, J. Zhuo, A. Forticaux, Z. Wang and S. Jin, *Chem. Mater.*, 2015, **27**, 5702-5711.
40. J. Wang, H. X. Zhong, Z. L. Wang, F. L. Meng and X. B. Zhang, *ACS Nano*, 2016, **10**, 2342-2348.
41. M. S. Faber, R. Dziedzic, M. A. Lukowski, N. S. Kaiser, Q. Ding and S. Jin, *J. Am. Chem. Soc.*, 2014, **136**, 10053-10061.
42. Q. Liu, J. Tian, W. Cui, P. Jiang, N. Cheng, A. M. Asiri and X. Sun, *Angew. Chem. Int. Ed.*, 2014, **126**, 6828-6832.
43. J. Tian, Q. Liu, A. M. Asiri and X. Sun, *J. Am. Chem. Soc.*, 2014, **136**, 7587-7590.
44. P. Jiang, Q. Liu, Y. Liang, J. Tian, A. M. Asiri and X. Sun, *Angew. Chem. Int. Ed.*, 2014, **53**, 12855-12859.
45. Z. Huang, Z. Chen, Z. Chen, C. Lv, H. Meng and C. Zhang, *ACS nano*, 2014, **8**, 8121-8129.
46. K. Xu, F. Wang, Z. Wang, X. Zhan, Q. Wang, Z. Cheng, M. Safdar and J. He, *ACS nano*, 2014, **8**, 8468-8476.
47. Q. Gong, L. Cheng, C. Liu, M. Zhang, Q. Feng, H. Ye, M. Zeng, L. Xie, Z. Liu and Y. Li, *ACS Catal.*, 2015, **5**, 2213-2219.
48. M. Cabán-Acevedo, M. L. Stone, J. R. Schmidt, J. G. Thomas, Q. Ding, H. C. Chang, M. L. Tsai, J. H. He and S. Jin, *Nat. Mater.*, 2015, **14**, 1245.
49. W. Liu, E. Hu, H. Jiang, Y. Xiang, Z. Weng, M. Li, Q. Fan, X. Yu, E. I. Altman and H. Wang, *Nat. Commun.*, 2016, **7**.
50. J. Zhuo, M. Cabánacevedo, H. Liang, L. Samad, Q. Ding, Y. Fu, M. Li and S. Jin, *ACS Catal.*, 2015, **5**.
51. K. Liu, F. Wang, K. Xu, T. A. Shifa, Z. Cheng, X. Zhan and J. He, *Nanoscale*, 2016, **8**, 4699-4704.
52. X. Zhan, Z. Wang, F. Wang, Z. Cheng, K. Xu, Q. Wang, M. Safdar and J. He, *Appl. Phys. Lett.*, 2014, **105**, 153903.
53. D. Kong, H. Wang, Z. Lu and Y. Cui, *J. Am. Chem. Soc.*, 2014, **136**, 4897-4900.
54. Z. Xing, Q. Liu, A. M. Asiri and X. Sun, *Adv. Mater.*, 2014, **26**, 5702-5707.
55. Q. Liu, J. Shi, J. Hu, A. M. Asiri, Y. Luo and X. Sun, *ACS Appl. Mater. Interfaces*, 2015, **7**, 3877-3881.
56. M. S. Faber, R. Dziedzic, M. A. Lukowski, N. S. Kaiser, Q. Ding and S. Jin, *J. Am. Chem. Soc.*, 2014, **136**, 10053-10061.
57. D. Kong, J. J. Cha, H. Wang, H. R. Lee and Y. Cui, *Energy Environ. Sci.*, 2013, **6**, 3553-3558.
58. M. Cabán-Acevedo, M. L. Stone, J. Schmidt, J. G. Thomas, Q. Ding, H.-C. Chang, M.-L. Tsai, J.-H. He and S. Jin, *Nat. Mater.*, 2015.
59. J. Zhuo, M. Cabán-Acevedo, H. Liang, L. Samad, Q. Ding, Y. Fu, M. Li and S. Jin, *ACS Catal.*, 2015, **5**, 6355-6361.
60. Y. Hou, M. R. Lohe, J. Zhang, S. Liu, X. Zhuang and X. Feng, *Energy Environ. Sci.*, 2016, **9**, 478-483.

View Article Online
DOI: 10.1039/C7NR00460E

Table of contents:

Varying compositions of ternary $CoP_{2x}Se_{2(1-x)}$ nanowires (NW) are synthesized via hydrothermal method followed by CVD method. Among them, $CoP_{1.37}Se_{0.63}$ NW needs overpotentials of only 70 mV and 98mV to achieve a current density of 10 mA/cm^2 in acidic and alkaline solution, respectively. This evidences the fact that this ternary material shows high catalytic activity in both acidic and alkaline condition.